

Characterization of Spatial-Temporal Channel Statistics from Measurement Data at D Band

Chathuri Weragama, *Student Member, IEEE*, Joonas Kokkonen, *Member, IEEE*,
 Mar Francis De Guzman, *Member, IEEE*, Katsuyuki Haneda, *Member, IEEE*, Pekka Kyösti,
 and Markku Juntti *Fellow, IEEE*.

Abstract—Millimeter-Wave (mmWave) (30-300 GHz) and D band (110–170 GHz) frequencies are poised to play a pivotal role in the advancement of sixth-generation (6G) systems and beyond with increased demand for greater bandwidth and capacity. This paper focuses on deriving a generalized channel impulse response for mmWave communications, considering both outdoor and indoor locations for line-of-sight (LOS) and non-line-of-sight (NLOS) scenarios. The analysis is based on statistical insights obtained from measurements conducted at distinct locations with a center frequency of 142 GHz, examining parameters such as path gain, delay, number of paths (NoP), and angle distributions. Whereas different distributions serve as candidate models for the gain of LOS communications, only specific distributions accurately describe the NLOS gain, LOS and NLOS delay, LOS and NLOS NoP, and LOS and NLOS angular distributions. The channel is modeled based on geometry-based stochastic channel modeling (GBSM) with parameters derived from the statistical analysis. The maximum excess delay is used as a metric to evaluate the performance of the proposed model against empirical data.

Index Terms—6G, channel measurement, channel model, D band, indoor measurements, outdoor measurements, maximum excess delay, millimeter-wave, statistical channels.

I. INTRODUCTION

IN the past decade, an exploration into millimeter-Wave (mmWave) frequencies up to 100 GHz has paved the way for their integration into fifth generation (5G) communication systems, offering improved communications, localization, and sensing catering to specific requirements within the industry [1]. However, the evolving demands of sixth generation (6G) communication, marked by higher data rates, seamless connectivity, and greater device density to support ultra reliable low latency communications (URLLC), massive machine type communications (mMTC), and enhanced mobile broadband (eMBB), necessitate a deeper investigation into propagation and channel characteristics at even higher frequencies. The D band, spanning from 110 GHz to 170 GHz, has emerged as a

focal point for addressing these requirements in 6G. Several studies have been carried out to understand the material characteristics and channel modeling at D band [2]–[5] considering reflection, scattering and diffraction phenomena at this frequency range. Whereas existing research has endeavored to characterize path loss, angular spread, and inter-cluster characteristics at the D band using indoor measurements [6], [7], challenges on channel modeling persist due to frequency-selective molecular absorption, high attenuation, reduced penetration through solid objects, and diffuse scattering [8]. The short wavelengths in the D band cause increased scattering from objects that are considered smooth at lower frequencies [9], further increasing the complexity of multipath modeling for mmWave communications.

One versatile technique for channel characterization is stochastic modeling, as it can capture the statistical behavior of wireless channels for different scenarios [10]. An extension of stochastic channel models, geometry-based stochastic channel model (GBSM) combines geometric and stochastic methods to formulate a channel model. By considering the relative geometries of link-ends and wave interaction objects, GBSM enables more generalized channel models for different environments operating in the same frequency compared to purely stochastic models. This contrasts with two other methods: deterministic channel modeling [11], [12], which focuses on specific environments, and hybrid channel modeling [13]–[15], which combines deterministic and stochastic approaches. Saleh-Valenzuela (S-V) model [16], a stochastic channel model, has been the basis for development of GBSM for frequencies below 100 GHz communications [17], [18], enabling more generalized channel models. A channel model based on GBSM for a factory environment at 140 GHz has been derived in [19], we intend to derive a channel model which is applicable for a variety of different environments such as airports, shopping malls and open halls with the intention of providing a basic channel model for signal processing algorithm development. To address this, we extend our preliminary work [20] on indoor channel propagation characteristics in D band communications to provide a comprehensive analysis on mmWave communication channels for frequencies above 100 GHz. Our previous study focused on path gain, delay, and number of paths (NoP) for indoor environments. In this paper, we significantly expand the scope and depth of our investigation.

The major contributions of this study are three-fold to:

- 1) Present a detailed characterization of mmWave radio

This work was supported by the European Union Smart Networks and Services Joint Undertaking (SNS JU) under grant agreement no. 101096949 (TERA6G). This research was also supported by the Research Council of Finland (former Academy of Finland) 6G Flagship Programme (Grant Number: 346208).

Chathuri Weragama, Joonas Kokkonen, Pekka Kyösti, and Markku Juntti are with Centre for Wireless Communications (CWC), University of Oulu, 90014 Oulu, Finland (email: chathuri.weragama@oulu.fi, joonas.kokkonen@oulu.fi, pekka.kyosti@oulu.fi, markku.juntti@oulu.fi)

Mar Francis De Guzman and Katsuyuki Haneda are with Department of Electronics and Nanoengineering, Aalto University School of Electrical Engineering, 02150 Espoo, Finland (email: francis.deguzman@aalto.fi, katsuyuki.haneda@aalto.fi)

propagation for both indoor and outdoor locations. This analysis reveals novel insights into the behavior of path gain, delay, and NoP across diverse environments, providing valuable data for the design of future mmWave systems.

- 2) Develop a channel impulse response for multiple-input multiple-output (MIMO) mmWave communications based on the GBSM. This model offers a versatile tool for researchers and engineers to accurately simulate and predict mmWave channel behavior in various scenarios.
- 3) Identify and discuss the specific benefits and limitations of deriving channel statistics solely from measurement data. This contribution provides crucial insights for researchers, highlighting areas where measurement-based approaches excel and where they may fall short, thus guiding future research methodologies in mmWave channel modeling.

Insights into statistical parametrization of mmWave channels are obtained based on measurements carried out in different indoor and outdoor locations. We characterize the path gain, delay and NoP parameters for indoor and outdoor radio links under line of sight (LOS) and non-line of sight (NLOS) conditions. A detailed analysis on angle of arrival (AoA)/ angle of departure (AoD) was conducted in [21] for the same data set. The mentioned channel parameters related to the collected data undergo comparisons with theoretical distributions to elucidate their inherent properties. We aim to aggregate all measured paths observed from specific locations to derive statistical distributions for amplitude or path gain, delay, and the NoP. The distributions, combined with the distribution of angular spread, a predetermined antenna array configuration, and free space path loss (FSPL) will make it possible to generate random wideband MIMO channel by arbitrarily summing paths from the derived distributions.

This paper is organized as follows. Section II provides a description of the channel model we will be using in our study and Section III provides an overview of the channel sounding procedure, while Section IV delineates the methodology employed for post-data processing of the measured channels and analysis of statistical parameters. Section V presents the findings of our analysis and associated statistical metrics, while Section VI provides verification and discussion on the results of this analysis. Finally, Section VII encapsulates the conclusions drawn from our study.

II. GEOMETRIC STOCHASTIC CHANNEL MODEL

Channel models can be determined for several purposes with various granularities. The simplest case is for predicting the overall signal attenuation, i.e., path loss modelling [22]–[25]. These are based on fitting a path loss curve over the measurement data and using a random variable to model fading/shadowing. For other needs, delay, spatial, and Doppler domains can also be considered. For MIMO modelling, typically channel impulse responses or transfer functions are to be predicted per transmitter (Tx)/receiver (Rx) antenna port pair. Path loss modelling using omni-directional assumption is

not applicable at the considered radio frequencies, since high antenna gains are a necessity on any practical systems, leading to highly directive antenna systems, i.e., strongly non-uniform antenna patterns.

A. Channel Model

We aim at deriving the statistics of the channels by deriving impulse response or transfer functions per Tx/Rx pair combining the antenna array patterns, where we analyse the characteristics of each multi-path component (MPC) of the channel in order to estimate the channel statistics. Our ultimate goal is to derive stochastic MIMO channel models by utilizing the statistics obtained from the measurements. While a similar approach to MIMO channel modeling has been undertaken in [26], it is noteworthy that our statistics are derived solely from measurement data. The GBSM for mmWave communications presented in this study is an extension of the S-V channel model, but without clustering, which differs to the channel model used in [19]. This channel model can be expressed mathematically as:

$$\mathbf{H} = \sum_{l=1}^L \delta_l^F(f, \tau_l) \delta_l^A \mathbf{a}_t(\phi_l) \mathbf{a}_r^H(\theta_l) e^{-i(2\pi f \tau_l + \beta)}, \quad (1)$$

where L is the number of paths, δ_l^F is the free-space propagation gain of the l^{th} path, which depends on the random delay (τ_l) of the path. δ_l^A is the excess path gain of the l^{th} path, which is dependent on the environment, $\mathbf{a}_{t/r} = A_o [1 e^{-j2\pi \sin(\theta/\phi + \theta_l/\phi_l)} \dots e^{-j2\pi(N_{T/R}-1) \sin(\theta/\phi + \theta_l/\phi_l)}]^T$ is the uniform linear array (ULA) response vectors, where $N_{T/R}$ is the number of antennas, A_o is a complex amplitude representing the antenna gain, which in a general case depends on the antenna radiation pattern and it is a vector if the antenna amplitudes are not equal or are adjustable. The departure and arrival angles of a path seen from the phase center of the antenna array are represented by θ_l and ϕ_l . It is worth noting that this antenna array response will be a scalar when a single-input single-output (SISO) scenario is considered. The last exponential term represents the phase shift experienced by the signal. For narrowband transmissions, this phase can be treated as entirely random for each path, since the frequency-dependent part ($2\pi f \tau_l$) doesn't vary much across the small bandwidth, and it combines with the random phase offset β . However, for wideband channels, we must explicitly consider the frequency dependency of this term ($2\pi f \tau_l$) across the larger bandwidth, as it leads to different phase shifts for different frequency components of the signal. The β term may still be random, but the overall phase ($2\pi f \tau_l + \beta$) behavior is dominated by the frequency-dependent term in wideband scenarios. A similar channel model has been used in recent signal processing research [27], [28].

B. Parameters of the Model

A proper understanding on the behaviour of path gain, delay, NoP, and the AoA/ AoD are required to derive a channel model based on (1). Once the AoA and AoD are determined, the antenna array response can be predetermined based on the

antenna type. FSPL can be calculated with the delay of the paths known. We aim to determine the statistical behaviour of these parameters related to mmWave communication based on measurement data with the intention of deriving a channel matrix for mmWave communication based on (1). An analysis on path gain, delay and NoP is performed in this study to understand the distribution of these parameters, as a detailed analysis on AoA/ AoD is performed in [21] for the same data set concluding these parameters follow a log-normal distribution. Once the distributions of the aforementioned parameters are identified we select random values from these distributions to build the channel model presented in (1).

It is important to note that the GBSM model presented in this study is based solely on measurement data, which introduces certain limitations. For instance, due to the finite number of available measured radio links, it is challenging to analyze whether the path gain and delay can be represented as a joint distribution. This analysis would require the very large number of link measurements that are difficult to obtain by the setup of sub-THz channel sounder in this paper. Potential solution would be to calibrate ray tracing simulators with real measurement data and then use simulated data to inflate the dataset and therefore get more data for the joint distribution analysis. However, this is out of scope of this work. Furthermore, the limited number of radio link measurements constrained our ability to draw definitive conclusions for distributions of some parameters, such as NoP. These limitations highlight the challenges inherent in developing comprehensive channel models based on empirical data and underscore the need for ongoing research and data collection in this field.

In the following section, we present a comprehensive set of channel measurements conducted across various indoor and outdoor locations. These measurements will allow us to examine the practical phenomenon of the channel characteristics outlined in our theoretical model, including path gain, delay, and the NoP.

III. CHANNEL MEASUREMENT DATA

The channel measurements on the D band were conducted by Aalto university in various locations in Helsinki region, Finland [29]–[31]. Several datasets from these measurements are openly available in [32]. The chosen indoor locations comprise commercial buildings: Sello shopping mall in the city of Espoo, Helsinki-Vantaa Airport, and the entrance hall of Aalto University in Espoo. Notably, measurements at the Aalto University entrance hall were collected during two separate periods, and treated as distinct locations for analysis purposes. Outdoor locations consist of Aalto University campus area, Helsinki city center area and Espoo city residential area.

All indoor locations have a relatively open floor plan with also some notable differences. The shopping mall is a multistory building with open areas but also more closed ones. The airport is mostly a single floor, but very open, and the Aalto university location is partially open space, but with more obstacles and features. When outdoor locations are considered, the campus area can be considered as a suburban area where

walls of the buildings in the area are mainly made up of bricks and have glass windows and doors with metallic frames. The Helsinki city center area is surrounded by commercial buildings forming a street canyon. The residential area is similar to the city center area but less dense with buildings. A detailed descriptions of these locations are provided in [33]. However, unlike the indoor locations the outdoor location measurements were conducted while moving objects were present in these locations.

The exact measurement setups have been detailed in various previous works, such as in [29] for the Aalto University entrance hall, [30] for the shopping mall, and [31] for the airport and shopping mall. The shopping mall and airport measurements were conducted at 143.1 GHz center frequency, while the remaining ones were conducted in the 142 GHz frequency with 4 GHz bandwidth. The Tx end was biconical omnidirectional antenna (0 dBi) and the Rx end was a horn antenna on rotating platform (19 dBi). The radio frequency (RF) power was about -7 dBm and the observed noise floor was -128 dBm, with an assumed margin of 10dB. The measurement details related to these seven locations are provided in Table I. In this table Sello, Airport, TUAS, and TUAS2 locations refer to Sello shopping mall, Helsinki-Vantaa Airport, initial measurement campaign at the entrance hall of Aalto University, and the second measurements for indoor locations, respectively. While campus, city, and residential locations refer to Aalto University area, Helsinki city-center area and the Espoo-city residential area for outdoor locations.

The same measurement data has been analysed before with respect to the fading statistics [34]. Our work here differs from that by aggregating the data per location in order to obtain statistically independent distributions (within the limits of the amount of measurement data available) as any single measurement link is strongly related to the environment geometry. When aggregating all the measurement positions per measurement location, we will obtain a stochastic data set as possible given the limitations of the real world measurements. The process of obtaining the statistics and channel modeling is described in the next section.

IV. MODELLING METHODOLOGY

A. Data Manipulation

We focus on analyzing the power delay profile (PDP), path gain distribution, delay distribution, and the NoP for both LOS and NLOS scenarios with the objective of modeling a channel frequency response for the D band communication. An analysis of angular spread of the MPCs has been carried out for the same data in previous studies [21], which suggests that it follows a log-normal distribution.

The data collection process discussed in Section III involved aggregating all MPCs observed from radio channel measurements in the measurement location into a unified dataset. Following this approach, the channel data underwent normalization of the FSPL for the gain estimates of MPCs based on the estimated delay of the same MPCs. This then mitigates the influence of distance and allows to examine power and delay distributions of MPCs. This way the free space expansion of

TABLE I
DETAILS ON MEASUREMENT CAMPAIGN

Measurement Details	Sello	Airport	TUAS	TUAS2	Campus	City	Residential
RF(GHz)	141.5-145.1	141.5-145.1	140-144	140-144	140-144	140-144	140-144
Tx Antenna Height(m)	1.89	1.7 above 2nd floor	1.85	1.85	1.85	1.85	2.00
Rx Antenna Height(m)	1.89	2.1 above 3rd floor	1.85	1.85	1.85	1.85	1.85
EIRP(dBm)	-12	-12	5	5	5	5	5
Rx Azimuth Range($^{\circ}$)	0-360	0-12, 245-360	40-250	-90-180(Rx1) 40-250(Rx2) 110-290(Rx3)	0-355	Mostly 0-355	Mostly 0-355
Azimuth Step($^{\circ}$)	6	5	10	5	5	5	5
Environment Type	Indoor	Indoor	Indoor	Indoor	Outdoor	Outdoor	Outdoor
Link Distance Range(m)	3-65	15-51	3-47	3-66	2-172	20-175	10-178

the waves is neglected and we can extract the loss related only to wave-object interaction. That is, we obtain the loss due to reflections, scattering, diffraction, multiple bounces, etc. to calculate the excess propagation loss. From this, we can calculate the statistics of the excess loss and add the free space loss back later when the path gain of MPCs is needed. Hence, this method aims to treat the far away paths equally to derive more accurate statistics for the excess loss.

The normalized received path gain, compensating for FSPL and obtain only the impact of the channel on the received power, is expressed as

$$P_{n(\text{dB})} = P_{(\text{dBm})} - 20 \log_{10} \left(\frac{4\pi f d}{c} \right), \quad (2)$$

where $P_{n(\text{dB})}$ denotes the normalized power, $P_{(\text{dBm})}$ is the measured power, and d , f , and c represent the length of the path, operating frequency, and speed of light in free space, respectively. The delay, on the other hand, is normalized with the delay of the first arrival to model the delay spread with the distributions. The normalization of delay was calculated as

$$\tau_n = \tau_l - \tau_1, \quad (3)$$

where τ_n , τ_l , and τ_1 correspond to the normalized delay, measured delay of the l^{th} MPC, and the delay of the first-arrived path, respectively. Modeling the NoP poses challenges due to inherent sparsity in the measurements. However, despite these challenges, we were able to derive reasonably accurate statistics for the NoP as well. This normalized power and delay data elucidate the behavior of power and delay profiles within the D band.

B. Analysis of Distributions

This analysis mainly focuses on deriving statistical distributions to represent path gain, delay, and NoP based on measured data. Throughout this analysis, we treat path gain and delay distributions independently of one another due to two main reasons.

- High losses prevent signals from bouncing indefinitely, hence the power and delay are less connected than in low frequency bands where large numbers of interactions lead to longer paths.
- The amount of data is too low to perform reliable joint distribution statistics. Producing such high amounts of

data is very challenging at these frequencies, because omnidirectional measurements are in practice not possible and directional measurements are always slower to perform.

To evaluate the statistical distributions derived from our measured data, we employed several analytical techniques. There are three main approaches to analyse the adequacy between the empirical and theoretical distributions, namely graphical methods, formal tests and normality tests. However, evaluating the goodness of fit of a distribution based on single evaluation metrics will lead to inaccurate results. Therefore, we have used both graphical and normality tests for our evaluation. When the normality tests are considered, we have evaluated many normality tests, including Kolmogorov-Smirnov (KS) test [35], the Kullback-Leiber (KL) divergence [36], Shapiro-Wilk, Lilliefors and the Anderson-Darling (AD) test. Though the literature suggests [37] that the AD test has a superior performance in comparison to KS test, since there are a number of distributions under consideration, KS test was used as the normality test due to its applicability in various distributions. The KS test statistic for a given m ordered data points is defined as

$$T = \sup_x |F_m(x) - F(x)|, \quad (4)$$

where \sup_x is the supremum of the set of distances, $F_m(x)$ is the empirical cumulative distribution function (CDF) and $F(x)$ is the CDF of the theoretical distributions. A p-value is calculated based on KS statistic and if the p-value exceed the critical value with respect to its significant value it is considered that the theoretical distribution is a good fit for the empirical distribution and vice versa. For visual representations, we have used both Q-Q plots and visualisation of CDFs (Figures 3 to 14) of theoretical and empirical distributions for our evaluation. Q-Q plots compare the quantiles of the first dataset against those of the second dataset. A perfect match between datasets from the same distribution would result in a plot following a $y = x$ line with a correlation coefficient of 1. We have used the correlation coefficient of this plot to serve as a metric for assessing the congruence between the two distributions.

TABLE II
NUMBER OF DATA POINTS PER LOCATION

Location Type	Location	LOS		NLOS	
		NoD	NoM	NoD	NoM
Indoor	Sello	304	16	29	2
	Airport	375	10	41	1
	TUAS	29	5	378	21
	TUAS2	268	16	1812	61
Outdoor	Campus	924	35	14	8
	City	768	12	435	21
	Residential	477	21	183	27

C. Maximum Excess Delay

The maximum excess delay (MED) can be used as a metric to evaluate the performance of our model against the empirical data. The MED of a channel can be calculated as

$$\tau = \tau_L - \tau_1, \quad (5)$$

where τ_L and τ_1 represents the delay of the last arriving MPC and the delay of the first arriving MPC respectively. To calculate the MED using the model as mentioned above, we have randomly drawn values for delay and gain from the respective distributions, which we have analysed for each scenario, and then calculated the power for each MPC by adjusting the gain for FSPL which was calculated based on the delay. Once the power values have been calculated we have drawn the delay components of the MPCs which have power values above the noise floor of the measurements. Once these delay values have been found we calculate the MED of the MPCs according to (5). Then these values were compared to the empirical MED for each location. The analysis of this study has been conducted in a Python environment using libraries numpy [38], pandas [39], and scipy.stats [40] for data manipulation, data organization and statistical fitting, respectively. The main tools that aided the visual representations of the said analysis are the matplotlib [41] and the seaborn [42] libraries. It is worth noting that statistical parameters related to distribution fitting in this study are compatible with Python scipy.stats library.

V. STATISTICAL CHANNEL PARAMETERS

As mentioned in Section IV, the data was collected for both indoor and outdoor locations covering LOS and NLOS propagation scenarios. This section discuss the results of the analysis conducted on these locations together with the statistics related to the analysis. The number of measurements (NoM), and the number of data points (NoD) for each location is presented in Table II. As discussed in the previous section, Sello, Airport, TUAS, and TUAS2 locations refer to Sello shopping mall, Helsinki-Vantaa Airport, initial measurement campaign at the entrance hall of Aalto University and the second measurements respectively for the indoor locations and for outdoor locations Campus, City, and Residential referees to Aalto University outdoor area, Helsinki city area and residential area of Espoo. We have analysed the measurements of MPCs based on location to understand the behaviour of power, delay, and NoP when propagating at D band.

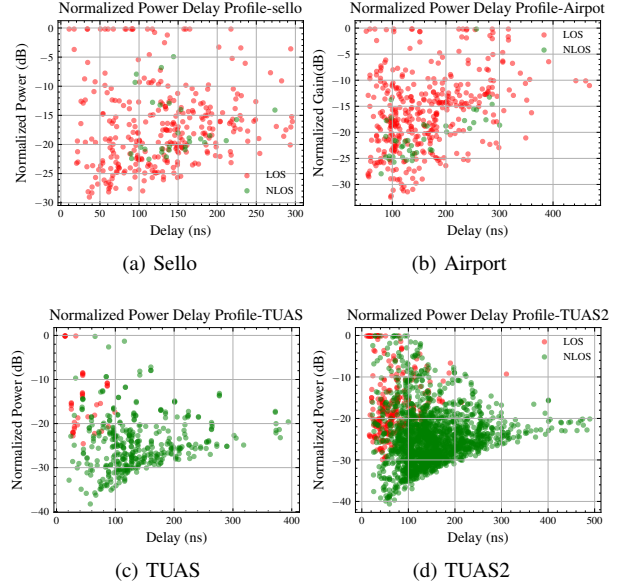


Fig. 1. Normalized power delay profile of indoor locations.

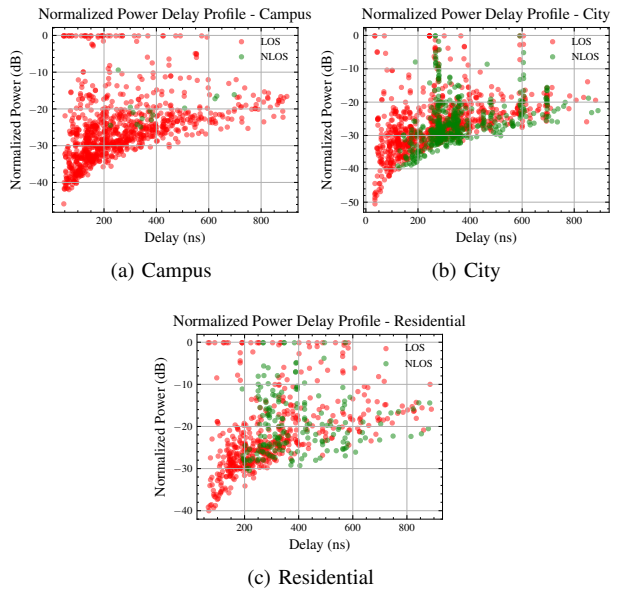


Fig. 2. Normalized power delay profile of outdoor locations.

A. Power Delay Profile

The PDP plays a pivotal role in understanding the behaviour of MPCs propagation in D band, as it provides a proper understanding on how the power of MPC components vary with the time of arrival with phenomena such as diffraction, scattering, and reflection available in the D band. We have analysed the normalized power according to (2), against the measured delay to eliminate the impact of FSPL. Figs 1 and 2 presents the PDP of indoor and outdoor locations respectively.

By observing the PDP of indoor and outdoor locations, it is evident that the PDPs follow the same pattern for both scenarios. There are several data points with 0 dB power indicating that the only loss available in these locations were FSPL. In general, these data points should appear in LOS measurements.

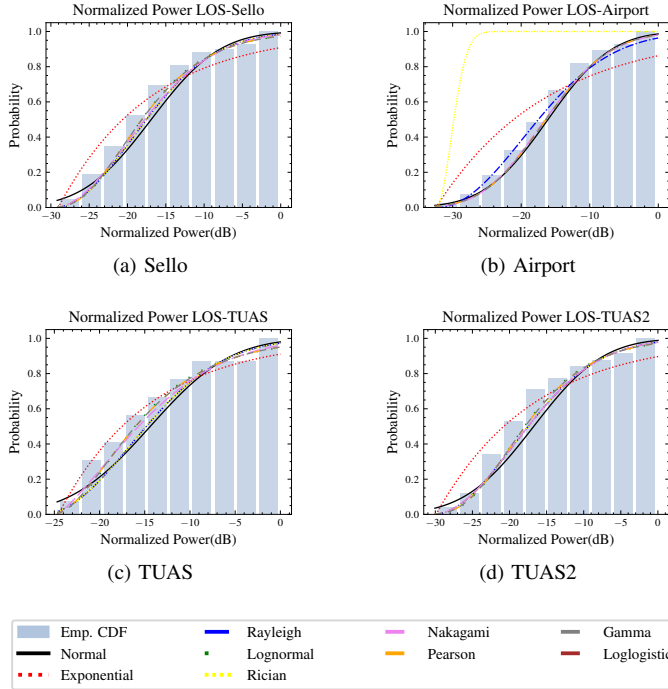


Fig. 3. Normalized power distribution for line-of-sight scenario in indoor locations.

However, interestingly it is visible that there are several NLOS data points with 0 dB power after normalization implying that there are LOS paths in even in NLOS scenarios. The reason for these data points could be that there are strong reflecting surfaces which will allow the signal to propagate to the receiver with almost zero excess loss in the signal. Further, when we analyze the PDP of locations with higher number of data points, such as TUAS, and TUAS2 for indoor, campus, residential, and city for outdoor we can observe a clear lower bond in the PDP. This can be an outcome of the environmental noise dominating over the received power when the transmission distance is high, and the system's inability to capture it due to the limitation of its dynamic range.

B. Normalized Power Distribution (NPD)

To perceive the distribution of normalized power of MPC components, we have analyzed the empirical distribution of the measured data against a set of candidate theoretical distributions to test the compatibility between the two distributions. As mentioned earlier, we have utilized both visual and normality tests to verify the goodness of fit of these distributions. Since the KS test compares the CDF of the two distributions, we have utilized the CDF for visual inspections as well. Furthermore, we have calculated the correlation coefficient with respect to Q-Q plots to understand the compatibility of the two distributions concerning the plots. Figures 3 to 6 present the normalized power distribution (NPD) of LOS and NLOS scenarios for indoor and outdoor measured values, and summary statistics related to distribution fitting and KS tests are provided in Appendix A.

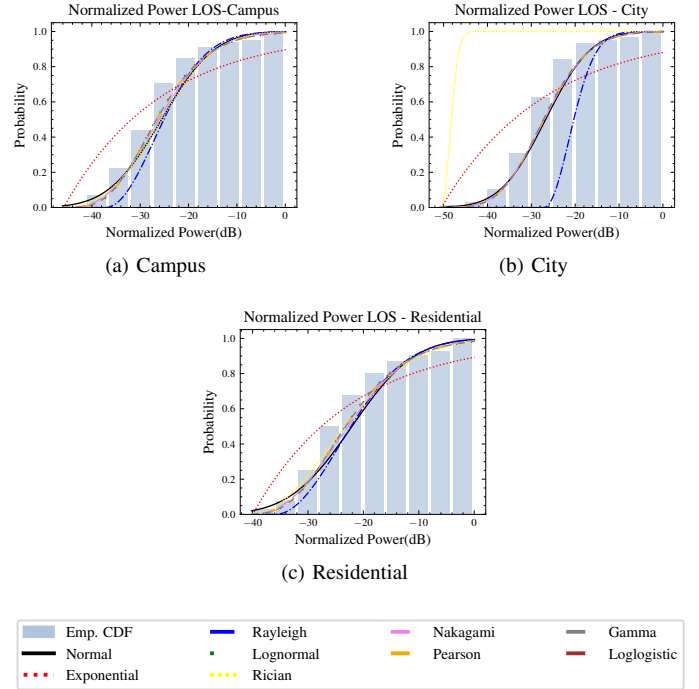


Fig. 4. Normalized power distribution for line-of-sight scenario in outdoor locations.

When we examine both visualizations and goodness of fit statistics in this analysis, it is challenging to effectively fit distributions for locations that have low numbers of data points/paths, such as LOS-TUAS, NLOS-Sello, NLOS-Airport and NLOS-City. The p-values associated with most distributions in these locations either exceed the significance threshold or has very low p-values, indicating insufficient evidence to reject or accept the null hypothesis of goodness of fit. However, visual inspection suggests that many distributions do not fit the data well in these locations. This discrepancy highlights the limitations of relying solely on statistical measures, especially in cases where the dataset size is small. Nevertheless, considering the entirety of visualizations and goodness of fit statistics reveals that several distributions, including **log-normal**, **Nakagami**, **gamma**, and **beta** distributions, exhibit satisfactory conformity with the LOS scheme for the indoor scenarios while **log-normal** and **gamma** distributions had a better fit when outdoor scenarios were considered. Notably, these distributions demonstrate acceptable values for both p and R values, indicating their suitability for modeling LOS propagation characteristics when a considerable number of data points are available. Conversely, in the case of the NLOS scheme, the data aligns well with the **log-logistic** distribution for indoor scenarios, particularly when a significant number of data points are available. When outdoor scenarios are considered the **log-normal** distributions seems to be the best fit for all three locations.

C. Normalized Delay Distribution

To anticipate the delay distribution of the multipath components at D band we have plotted the CDFs related to the

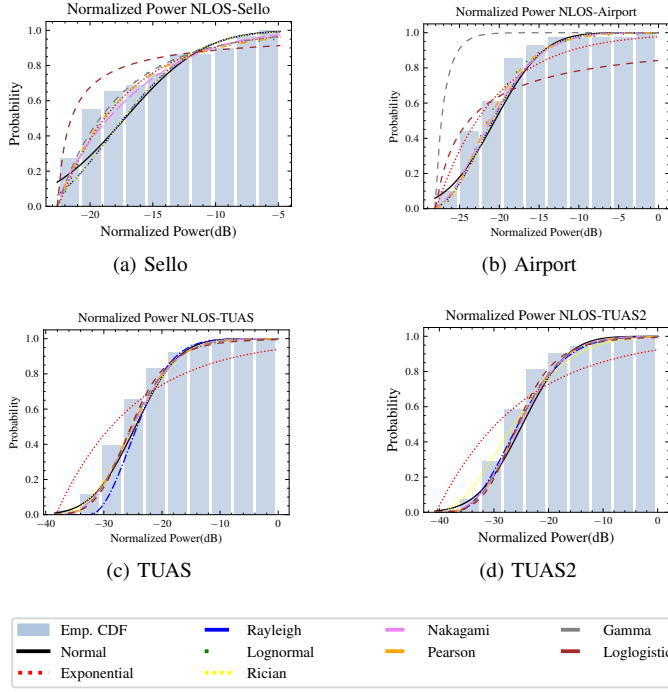


Fig. 5. Normalized power distribution for non-line-of-sight scenario in indoor locations.

normalized delay as stated in (3) and compared the results with different theoretical CDFs. The resulting graphs are presented in Figures 7 to 10; the summary statistics related to the distribution fitting and KS test are presented in Appendix B.

Similar to the challenges encountered in fitting the distributions to the NPD, the normalized delay distribution (NDD) also presents corresponding difficulties, particularly when the number of data points is low. However, unlike the NPD, the NDD reveals a limited number of distributions suitable for empirical fitting. Specifically, the Weibull and exponential distributions emerge as potential candidates for modeling the NDD behavior. Upon comprehensive analysis of statistics and visualizations, it becomes evident that the **exponential** distribution emerges as the most suitable fit for both LOS and NLOS schemes for both indoor and outdoor locations within the NDD framework. It offers the most accurate representation of delay characteristics in both LOS and NLOS scenarios despite the challenges posed by limited dataset sizes.

D. The Number of Paths

To discern the NoP in D band indoor and outdoor wireless channels, we have analysed the data in two perspectives. Firstly, we have analysed the NoP to examine which distribution best fits the empirical data, similar to the analysis in [43]. Secondly, we have analysed the NoP captured for each distance measurement between the Tx and the Rx. The visualizations related to this analysis are presented in Figures 11 to 18. The maximum, minimum, and mean of NoPs for each location are provided in Table III, and summary statistics of the KS test for different distributions applied to this data set are provided in Appendix C. For the LOS scenario,

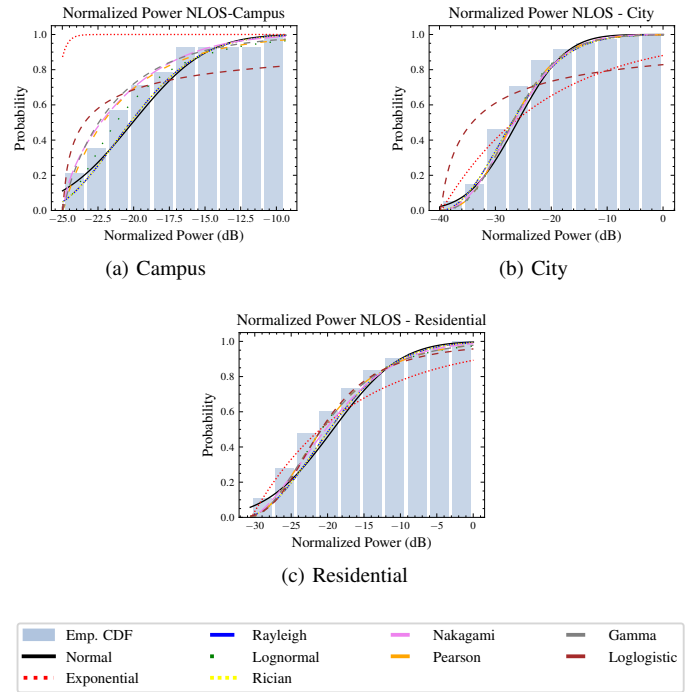


Fig. 6. Normalized power distribution for non-line-of-sight scenario in outdoor locations.

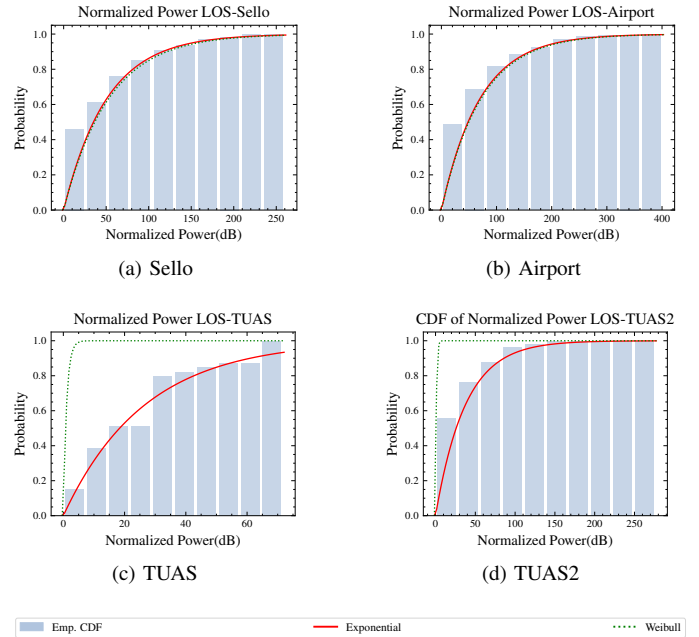


Fig. 7. Normalized delay distribution for line-of-sight scenario in indoor locations.

we considered the Sello, Airport indoor locations and Campus, Residential outdoor locations. TUAS, TUAS2 and City, Residential locations were selected for the NLOS scenario for indoor and outdoor locations respectively. This location selection was based on the highest number of measurement points available as mentioned in Table II.

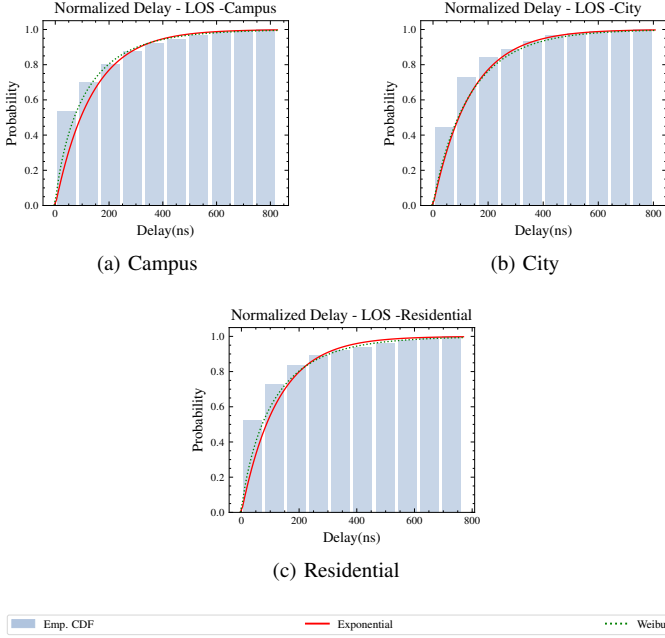


Fig. 8. Normalized delay distribution for line-of-sight scenario in outdoor locations.

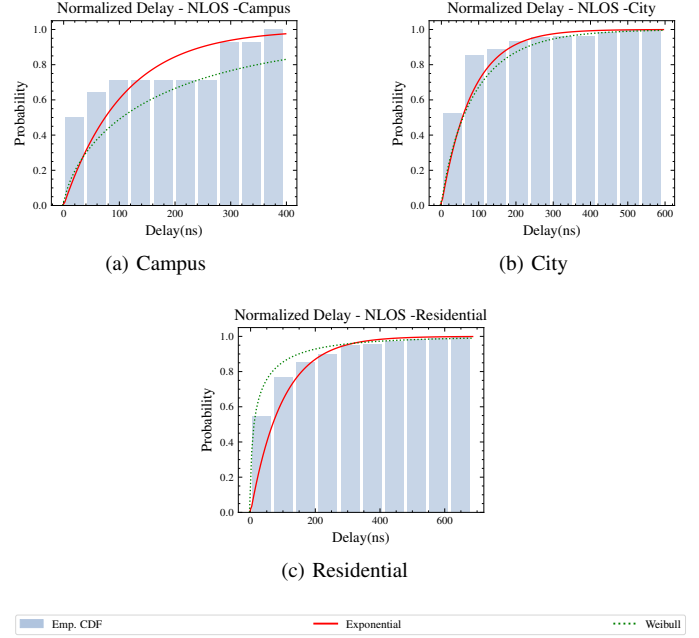


Fig. 10. Normalized delay distribution for non-line-of-sight scenario in outdoor locations.

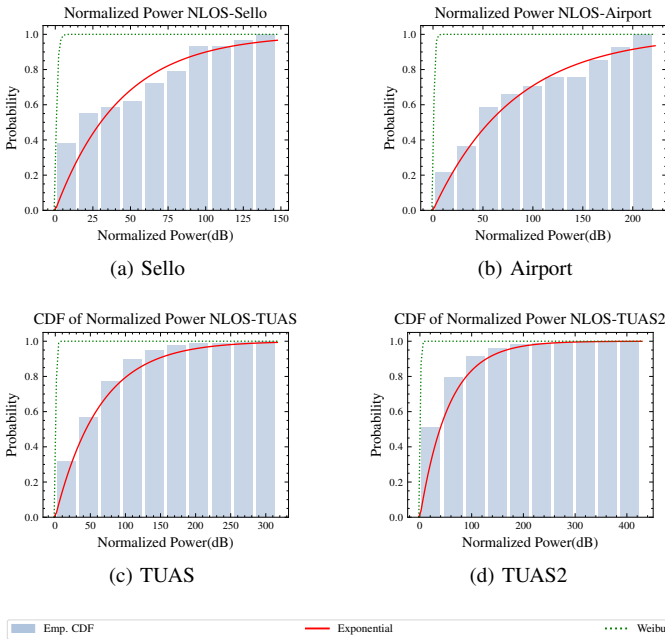


Fig. 9. Normalized delay distribution for non-line-of-sight scenario in indoor locations.

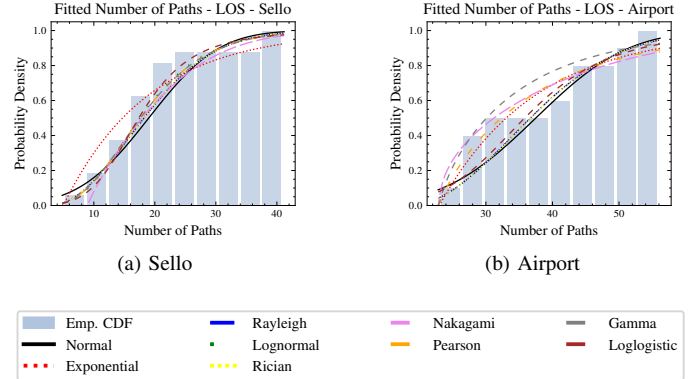


Fig. 11. Distribution of MPCs for line-of-sight scenario in indoor locations.

By carefully examining the statistics of the goodness of fit, it is evident that log-logistic distribution best describes the distribution of the NoP when the LOS scenario is considered for both indoor and outdoor locations and normal distribution fits best when NLOS data are considered. However, when we cross examine the visualisations and the goodness of fit statistics it becomes evident that we cannot rely on these conclusions as they contradict with one another. The main cause for this

can be due to the lack of data points for this specific analysis as we are considering the number of measurement points as stated in Table II. Furthermore, the box plot visualizations of indoor locations (Figures 15 to 16) suggest that the median of NoP in indoor locations increases up to the 20 m – 30 m distance range, following which it begins to decline with the Tx-Rx separation. However, considering the indoor dataset, a consistent trend is evident. The median NoP peaks when the Tx-Rx distance falls within the 10 m – 30 m distance range for both LOS and NLOS scenarios. This phenomenon can be attributed to the positioning of the Tx and Rx creating very few short paths initially, while the NoP increases with increasing distance. Subsequently, when the Tx and Rx are further separated, the power of these components falls below a specific threshold due to the dynamic range of the system, becoming undetectable to the Rx. Unlike indoor locations, the median of NoP for outdoor locations increase with Tx-

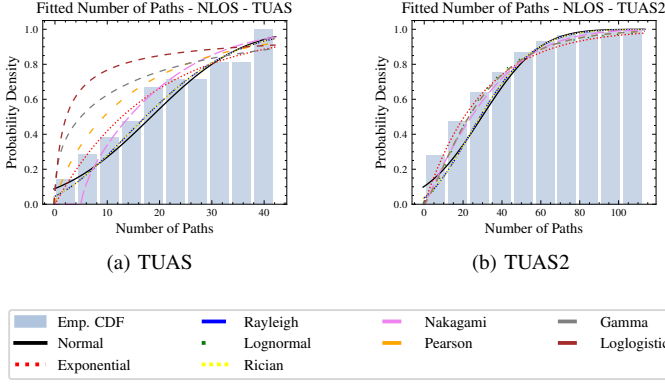


Fig. 12. Distribution of MPCs for non-line-of-sight scenario in indoor locations.

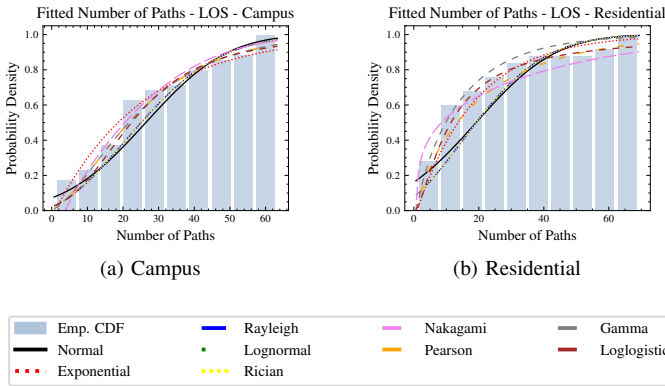


Fig. 13. Distribution of MPCs for line-of-sight scenario in outdoor locations.

Rx separation. This trend may be due to the tunneling effect created by the nature of the outdoor environment.

E. Angular Spread

A detailed analysis on angular spread for the same data set is presented in [21]. This analysis reveals that the angular spread only slightly decreases with the frequency band. Further, it is revealed that the angular spread follows a log-normal distribution and the statistics related to each location with a detailed analysis are provided in [21]. For the GBSM model provided in this study, we assume that the angular spread follows a log-normal distribution.

The statistical analysis presented in Section V provides valuable insights into the characteristics of mmWave propagation in the D band. To further validate these findings and assess the practical applicability of our proposed GBSM, the next section concentrates on model verification and a comprehensive discussion of the results.

VI. VERIFICATIONS AND DISCUSSION

In this section, we will first evaluate the performance of our GBSM by comparing its predictions against the empirical data, focusing particularly on the MED as a key performance metric. Following this verification, we will engage in a detailed

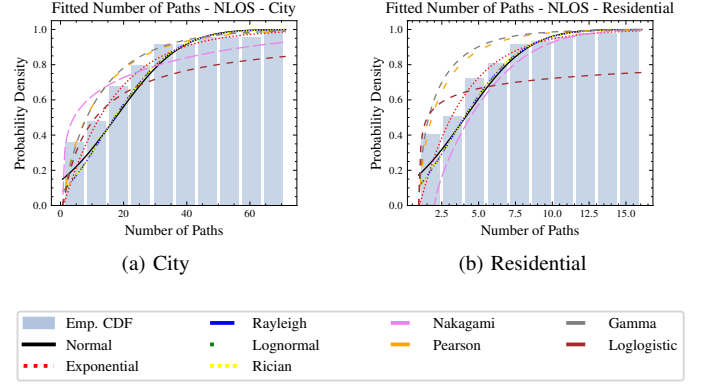


Fig. 14. Distribution of MPCs for non-line-of-sight scenario in outdoor locations.

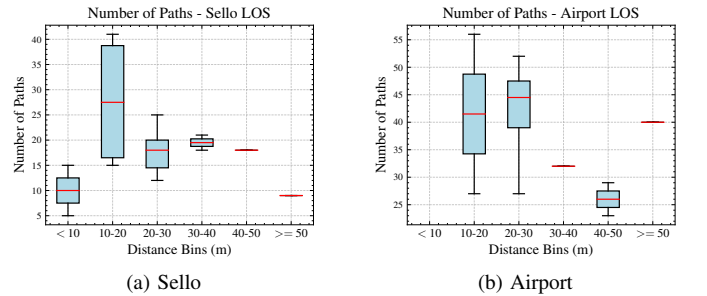


Fig. 15. MPCs vs. Tx-Rx distance for line-of-sight in indoor locations

discussion of our findings, exploring their implications for D Band communications.

A. Maximum Excess Delay

As mentioned in Section IV, we have used MED as a metric to evaluate the performance of our model against the empirical data. The detailed description of MED calculation based on this model is provided in Section IV-C. Although several candidate distributions were identified for the LOS scenario of NPD in both indoor and outdoor locations, we selected the log-normal distribution for both scenarios in this analysis, based on our consideration of both goodness-of-fit statistics and visualizations. The average MED of each location based on empirical data and the model is provided in Table IV. However, it's worth noting that we have not used any distribution to represent the number of paths, as the results of the analysis are inconclusive. Instead, the NoP value related to each measurement from the empirical data has been used. Further to the discovery of the accuracy of the model when compared to the empirical data, this comparison also highlights the impact of the number of data points throughout the analysis. As Figure 19 represents the two scenarios of the delay distribution of empirical and model data in reference to a scenario with higher number of data points and very low number of data points.

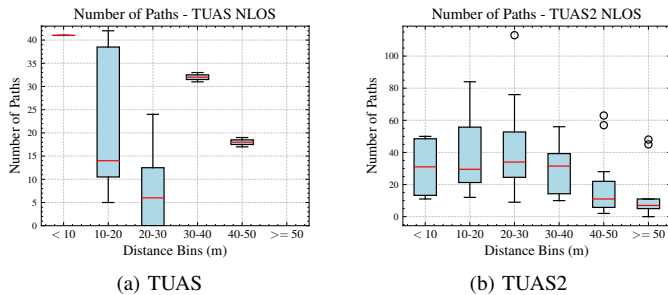


Fig. 16. MPCs vs. Tx-Rx distance for non-line-of-sight in indoor locations

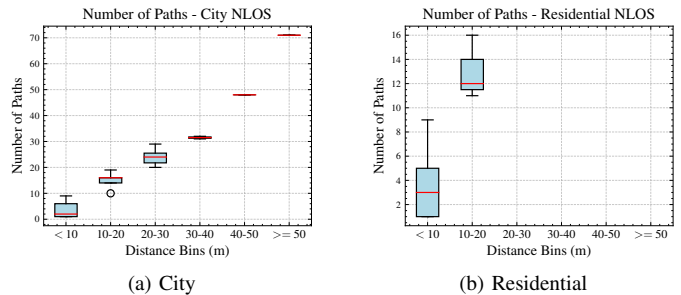


Fig. 18. MPCs vs. Tx-Rx distance for non-line-of-sight in outdoor locations.

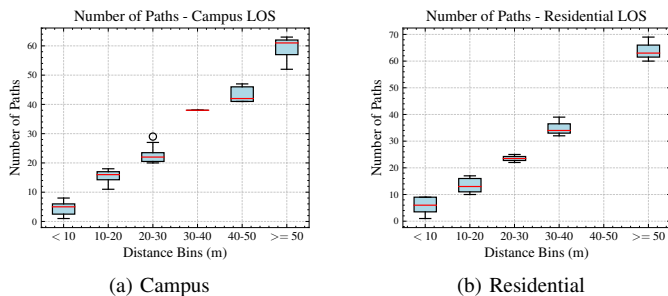


Fig. 17. MPCs vs. Tx-Rx distance for line-of-sight in outdoor locations.

B. Channel Modeling Based on Measurements

This study has focused on deriving channel statistics purely based on measurement data. There were both benefits and drawbacks to this method. The main benefit is the ability to model the real environment based on measurements rather than relying on assumptions about the environment. This enables more accurate channel characterization, leading to more precise channel modeling.

However, throughout this analysis, it was evident that there were a few scenarios with insufficient data points, leading to inconclusive results (e.g., NoP) and further we were unable to analyse specific connection between these parameters due to the same limitation. This is the main drawback of building channel models solely based on measurement data, as the measurement campaign can be time-consuming and may result in an inadequate number of data points for proper analysis.

C. Discussion

Upon reviewing the results, it becomes apparent that several distributions can be used to represent the NPD of the LOS-indoor scenario, while the log-normal and gamma distributions seems to be the best fit for the LOS-outdoor scenario. When the NLOS scenario is considered, the log-logistic distribution appears to be the only eligible candidate to represent the distribution of the NPD for indoor locations, while the log-normal distribution has the best statistics for outdoor locations. Unlike the NPD, in the NDD distribution analysis there are only a few candidate distributions that can be considered to represent the NDD distribution, namely the Weibull and exponential distributions. Among these two, the exponential distribution outperforms the Weibull distribution in all scenarios. Furthermore, discrepancies between the results of the

TABLE III
STATISTICS OF NUMBER OF PATHS

Location	LOS			NLOS		
	Max.	Min.	Mean	Max.	Min.	Mean
Sello	41	5	19	19	10	14.5
Airport	56	23	37.5	41	41	41
TUAS	11	6	7.8	42	0	18.5
TUAS2	49	6	16.8	113	0	29.7
Campus	63	1	26.4	4	1	2.25
City	178	8	64	71	1	17.48
Residential	69	1	19.16	16	1	4.01

KS test and Q-Q plots are noted. These inconsistencies may stem from the relatively low number of data points used in the analysis. The KS test's sensitivity to dataset size can lead to unreliable performance when data points are scarce, while Q-Q plots may tend to overfit small datasets.

When the number of MPC components per transmission is considered, it is difficult to arrive at a conclusion on a specific distribution for its distribution relying solely on the visual representations and the statistics of goodness of fit as they contradict with one another due to the lack of data points. However, when the number of MPCs are plotted against the Tx-Rx separation, a clear pattern can be observed in both indoor and outdoor locations for LOS and NLOS scenarios.

Considering indoor and outdoor locations, it can be observed that both scenarios have similar patterns in LOS transmission, with slight changes in the NLOS transmissions on NPD distributions. However, when the NoP per transmission is considered, it can be observed that the NoPs in outdoor locations is reasonably higher compared to indoor transmissions for LOS scenario, while the NoPs are lower in outdoor locations for the NLOS scenario. There can be two valid explanations for this. One is that the measurements of the MPC are captured below a 30 dB threshold from the strongest measured path. Since the Tx/Rx separation of the LOS outdoor scenarios is greater than that of the indoor locations, the strongest path of outdoor locations may have less power, resulting in a threshold that might capture more MPCs outdoors. Secondly, the indoor environments have more lossy interactions than outdoor environments, reducing the number of captured MPCs.

VII. CONCLUSIONS

In this paper, we derived a GBSM for mmWave communications above 100 GHz relying on spatial-temporal statis-

TABLE IV
COMPARISON OF EMPIRICAL DATA AND MODEL PREDICTIONS FOR
AVERAGE MED

Location	Scenario	Empirical MED (ns)	Model MED (ns)
Sello	LOS	155.2	113.2
	NLOS	-	-
Airport	LOS	276.56	240.78
	NLOS	-	-
TUAS	LOS	110.69	88.13
	NLOS	159.78	228.89
TUAS2	LOS	110.69	124.54
	NLOS	172.65	260.31
Campus	LOS	542.25	562.04
	NLOS	317.12	351.35
City	LOS	482.51	408.04
	NLOS	281.1	306.65
Residential	LOS	376.49	467.87
	NLOS	188.7	412.17

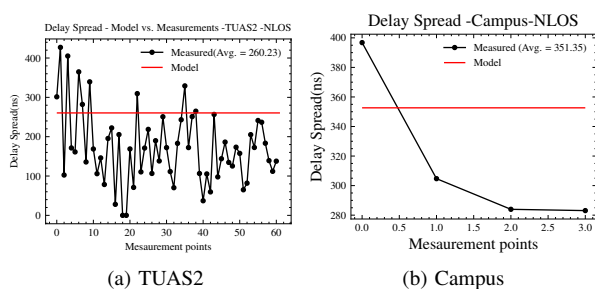


Fig. 19. Delay distribution comparison between the measured data and model predictions.

tics based on measurements conducted in the D band with the motivation of creating a generalized channel frequency response for MIMO communications in mmWave frequency. Specifically, a detailed analysis was conducted on path gain, delay, and the NoP, considering both LOS and NLOS scenarios for indoor and outdoor locations. Theoretical distributions were utilized to characterize the behavior of MPCs for path gain and delay in the D band. While several distributions accurately characterize the behavior of the LOS power distribution for indoor locations, other distributions, namely the NLOS power distribution for indoor locations characterized by log-logistic distribution, LOS and NLOS NPD for outdoor locations through log-normal as well as the LOS and NLOS delay distributions for all locations characterized by the exponential distribution, exhibit specific characteristics that can only be accurately captured by these relevant distributions. This comprehensive analysis, together with the analysis on angular spread has enabled us to arrive at a more accurate channel frequency response modeling for the mmWave frequency communication. To confirm the accuracy of our model, we have compared the MED of the synthetic data generated from the model against the empirical data which we gathered through measurements. Interestingly, we can observe that the model presented in this research provides acceptable results against the empirical data. However, this research also emphasizes the shortcoming of lack of measurement points for a detailed analysis motivating future research to be conducted on increased number of measurements for higher frequency

communications.

APPENDIX A NORMALIZED POWER DISTRIBUTION SUMMARY STATISTICS

Table V and VI provides the statistics related to the KS test – an estimate of the maximum distance between the two CDFs under testing, the p-value which provides a threshold for acceptance of the theoretical distributions, and the parameters: **loc** – shift of the distribution along the x-axis, **scale** – the standard deviation of the distribution, and the **shape** parameter which controls the skewness of the distribution while fitting the measured data to each candidate distribution for indoor and outdoor locations respectively.

APPENDIX B SUMMARY STATISTICS OF NORMALIZED DELAY DISTRIBUTION- (COMPATIBLE WITH PYTHON SCIPY.STATS LIBRARY)

Tables VII and VIII provided summary statistics of fitting different distributions for indoor and outdoor locations respectively. Unlike NPD, since the lowest delay encountered from the normalized delay distribution is zero we have forced each distribution to locate at zero.

APPENDIX C SUMMARY STATISTICS OF DISTRIBUTION OF NUMBER OF PATHS

Summary statistics of KS test on fitting different distributions to empirical data for NoP is provided in Tables IX and X for indoor and outdoor locations respectively.

TABLE V
SUMMARY STATISTICS OF THE NORMALIZED POWER DISTRIBUTION IN INDOOR LOCATIONS - (COMPATIBLE WITH PYTHON SCIPY.STATS LIBRARY)

Location	Distribution	LOS							NLOS						
		KS Stat	p-value	R	Loc	Scale	Shape	KS Stat	p-value	R	Loc	Scale	Shape		
Sello	Normal	0.081	0.033	0.97	-17	7	-	0.223	0.096	0.92	-17.2	4.93	-		
	Exponential	0.205	9×10^{-12}	0.97	-29	12.1	-	0.106	0.866	0.96	-22.5	5.31	-		
	Log-Normal	0.344	0.853	0.99	-35.5	17.4	0.37	0.120	0.751	0.91	-23.1	4.03	0.91		
	Rayleigh	0.048	0.446	0.99	-29.6	10.3	-	0.232	0.074	0.96	-24.9	6.48	-		
	Rician	0.048	0.446	0.99	-29.6	10.3	0	0.232	0.074	0.96	-24.9	6.48	0		
	Nakagami	0.046	0.524	0.99	-29.3	14.2	0.876	0.118	0.772	0.98	-22.5	7.26	0.88		
	Gamma	0.036	0.811	0.99	-30.7	3.73	3.66	0.103	0.721	0.98	-22.5	5.74	0.88		
	Beta	0.036	0.811	0.99	-16.9	7.14	1.04	0.127	0.883	0.98	-17.1	5.6	2.1		
Log Logistic	0.35	2×10^{-34}	0.57	-29	5.6	0.84	0.413	5×10^{-5}	0.58	-22.5	1.1	0.83			
Airport	Normal	0.036	0.689	0.99	-16.08	7.3	-	0.124	0.5092	0.92	-20.5	4.83	-		
	Exponential	0.26	2×10^{-24}	0.93	-32.4	16.3	-	0.241	0.014	0.97	-27.9	7.38	-		
	Log-Normal	0.029	0.884	0.99	-105.5	89.16	0.08	0.087	0.892	0.97	-30.9	9.4	0.42		
	Rayleigh	0.087	0.005	0.99	-32.2	16.3	-	0.105	0.715	0.96	-28.75	6.72	-		
	Rician	0.908	0	0.27	-32.4	2.2	0	0.105	0.715	0.95	-28.7	6.7	0		
	Nakagami	0.031	0.839	0.99	-41.2	26.1	3.04	0.09	0.864	0.96	-28.2	9.06	0.79		
	Gamma	0.029	0.892	0.99	-72.5	0.94	59.7	0.072	1×10^{-31}	0.97	-27.9	1.55	0.73		
	Beta	0.029	0.892	0.99	-16	7.31	0.26	0.827	0.971	0.97	-20.5	4.5	1.1		
Log Logistic	0.035	0.72	0.99	-102.7	86.3	20.6	0.334	7×10^{-5}	0.78	-27.9	4.14	0.88			
TUAS	Normal	0.115	0.635	0.95	-14.3	7	-	0.074	0.026	0.97	-24.5	5.8	-		
	Exponential	0.152	0.297	0.93	-24.5	10.1	-	0.320	7×10^{-36}	0.90	-38.2	13.67	-		
	Log-Normal	0.120	0.965	0.94	-28.2	12.1	0.52	0.027	0.923	0.96	-48.56	23.3	0.24		
	Rayleigh	0.107	0.725	0.97	-26.4	9.8	-	0.119	3×10^{-5}	0.96	-32.5	6.9	-		
	Rician	0.107	0.725	0.97	-26.4	9.8	0	0.06	0.112	0.96	-38.5	6.6	1.8		
	Nakagami	0.086	0.907	0.97	-24.7	12.4	2.1	0.048	0.381	0.96	-39.5	16.0	1.78		
	Gamma	0.069	0.958	0.96	-25.2	5.04	1.36	0.031	0.831	0.99	-42.47	1.88	9.50		
	Beta	0.069	0.958	0.96	-14.4	7.4	1.04	0.031	0.831	0.99	-24.5	5.8	0.64		
Log Logistic	0.04	2.3×10^{-5}	0.47	-24.6	3.3	0.81	0.01	0.969	0.99	-46.11	20.78	6.62			
TUAS2	Normal	0.126	3×10^{-4}	0.94	-16.7	7.3	-	0.084	9×10^{-12}	0.98	-24.63	6.5	-		
	Exponential	0.246	7×10^{-15}	0.90	-29.9	13.1	-	0.33	8×10^{-177}	0.24	-40.6	15.8	-		
	Log-Normal	0.059	0.283	0.98	-36.4	18.3	0.37	0.042	2×10^{-3}	0.98	-50.1	24.6	0.24		
	Rayleigh	0.093	0.017	0.98	-30.42	11	-	0.059	5×10^{-6}	0.98	-37.3	10	-		
	Rician	0.093	0.017	0.98	-30.42	11	0	0.142	3×10^{-32}	0.98	-40.6	12.1	0.11		
	Nakagami	0.093	0.018	0.98	-30.3	15.5	1	0.064	5×10^{-7}	0.97	-41.7	18.1	1.8		
	Gamma	0.069	0.146	0.99	-32.0	3.51	4.3	0.048	3×10^{-4}	0.98	-44.4	2.1	9.56		
	Beta	0.069	4×10^{-4}	0.93	-16.7	7.3	0.95	0.048	4×10^{-4}	0.98	-24.7	6.3	0.64		
Log Logistic	0.042	0.70	0.99	-33.7	15.5	4.04	0.017	0.878	0.98	-47.4	21.7	6.4			

TABLE VI
SUMMARY STATISTICS OF THE NORMALIZED POWER DISTRIBUTION IN OUTDOOR LOCATIONS- (COMPATIBLE WITH PYTHON SCIPY.STATS LIBRARY)

Location	Distribution	LOS							NLOS						
		KS Stat	p-value	R	Loc	Scale	Shape	KS Stat	p-value	R	Loc	Scale	Shape		
Campus	Normal	0.095	9×10^{-8}	0.96	-25.57	8.68	-	0.162	0.80	0.94	-25.57	8.68	-		
	Exponential	0.31	4×10^{-83}	0.97	-45.83	20.25	-	0.13	0.94	0.97	-45.83	20.26	-		
	Log-Normal	0.052	0.011	0.98	-55.03	28.28	0.28	0.115	0.98	0.98	-55.03	28.28	0.28		
	Rayleigh	0.107	8×10^{-10}	0.98	-37.17	10.24	-	0.14	0.90	0.98	-37.1	10.24	-		
	Rician	0.101	1×10^{-8}	0.96	-46.04	9.39	1.92	0.14	0.90	0.97	-46.04	9.39	1.92		
	Nakagami	0.078	2×10^{-5}	0.97	-46.57	22.72	1.66	0.21	0.50	0.97	-41.57	22.72	1.66		
	Gamma	0.060	0.002	0.98	-25.57	8.47	0.74	0.22	0.39	0.99	-48.56	3.12	7.36		
	Beta	0.060	0.002	0.98	-48.56	3.12	7.36	0.19	0.58	0.98	-25.57	8.47	0.73		
Log Logistic	0.690	0	0.49	-45.83	1.34	0.57	0.33	0.07	0.73	-45.83	1.34	0.57			
City	Normal	0.079	1×10^{-4}	0.97	-26.75	8.14	-	0.112	3.5×10^{-5}	0.96	-26.09	6.86	-		
	Exponential	0.37	3×10^{-93}	0.96	-50.50	23.75	-	0.3	3.51×10^{-5}	0.98	-39.66	13.56	-		
	Log-Normal	0.059	0.008	0.98	-85.46	58.16	0.13	0.059	0.087	0.99	-49.29	22.27	0.28		
	Rayleigh	0.59	1×10^{-254}	0.97	-27.09	5.76	-	0.099	3×10^{-4}	0.98	-39.85	10.86	-		
	Rician	0.98	0	0.97	-49.31	2.03	1.3	0.099	3×10^{-4}	0.98	-39.86	10.87	5×10^{-4}		
	Nakagami	0.07	9×10^{-4}	0.97	-62.62	36.78	5.07	0.08	6×10^{-3}	0.98	-40.65	16.09	1.3		
	Gamma	0.060	0.002	0.99	-32.0	3.51	4.3	0.048	3×10^{-4}	0.98	-44.4	2.1	9.56		
	Beta	0.062	0.005	0.98	-26.75	8.04	0.36	0.063	0.063	0.99	-26.09	6.7	0.76		
Log Logistic	0.027	0.59	0.98	-78.07	50.64	12	0.44	2×10^{-78}	0.67	-39.66	5.53	0.8			
Residential	Normal	0.11	8×10^{-6}	0.96	-22.05	8.86	-	0.10	0.045	0.97	-19.24	7.21	-		
	Exponential	0.29	4×10^{-38}	0.97	-40	17.95	-	0.1	1×10^{-4}	0.98	-30.47	11.23	-		
	Log-Normal	0.056	0.01	0.98	-50.82	27.49	0.3	0.05	0.69	0.99	-34.64	13.79	0.47		
	Rayleigh	0.107	8×10^{-10}	0.98	-30.42	11	-	0.059	5×10^{-6}	0.98	-31.75	10.21	-		
	Rician	0.111	1×10^{-5}	0.98	-40.19	21.07	1.31	0.081	0.165	0.99	-31.75	10.21	4×10^{-4}		
	Nakagami	0.08	3×10^{-3}	0.98	-41.17	21.07	1.31	0.04	0.83	0.99	-30.56	13.43	0.71		
	Gamma	0.062	0.045	0.99	-22.05	8.72	0.78	0.042	0.877	0.99	-31.13	4.73	2.51		
	Beta	0.062	0.045	0.99	-16.7	7.3	0.95	0.042	0.877	0.99	-19.24	7.5	1.26		
Log Logistic	0.039	0.42	0.98	-46.73	23.13	5.042	0.055	0.605	0.99	-33.02	12.13	3.1			

TABLE VII

SUMMARY STATISTICS OF THE NORMALIZED DELAY DISTRIBUTION IN INDOOR LOCATIONS- (COMPATIBLE WITH PYTHON SCIPY.STATS LIBRARY)

Location	Distribution	LOS					NLOS				
		KS Stats	p-value	R	Loc	Scale	KS Stats	p-value	R	Loc	Scale
Sello	Exponential	0.07	0.04	0.99	0	50.52	0.14	0.56	0.99	0	43.51
	Weibull	0.09	0.01	0.99	0	52.72	0.82	4×10^{-22}	0.91	0	1.05
Airport	Exponential	0.05	0.21	0.99	0	69.7	0.09	0.8	0.99	0	81.21
	Weibull	0.06	0.09	0.99	0	71.65	0.97	2×10^{-66}	0.90	0	1.05
TUAS	Exponential	0.17	0.16	0.99	0	26.5	0.09	0.002	0.99	0	63.2
	Weibull	0.84	4×10^{-32}	0.91	0	1.05	0.91	0	0.99	0	1.05
TUAS2	Exponential	0.06	0.28	0.99	0	37.5	0.05	0.0001	0.99	0	55.7
	Weibull	0.9	1×10^{-262}	0.99	0	1.05	0.61	0	0.99	0	1.05

TABLE VIII

SUMMARY STATISTICS OF THE NORMALIZED DELAY DISTRIBUTION IN OUTDOOR LOCATIONS- (COMPATIBLE WITH PYTHON SCIPY.STATS LIBRARY)

Location	Distribution	LOS					NLOS				
		KS Stats	p-value	R	Loc	Scale	KS Stats	p-value	R	Loc	Scale
Campus	Exponential	0.11	6×10^{-12}	0.99	0	136.2	0.33	0.06	0.91	0	107.38
	Weibull	0.057	4×10^{-4}	0.99	0	136.19	0.05	0.004	0.99	0	109.93
City	Exponential	0.04	0.10	0.99	0	135.25	0.103	1×10^{-4}	0.95	0	81.05
	Weibull	0.05	0.02	0.99	0	139	0.17	1×10^{-11}	0.95	0	97.87
Residential	Exponential	0.08	2×10^{-3}	0.99	0	124.89	0.21	1×10^{-7}	0.96	0	98.05
	Weibull	0.13	5×10^{-8}	0	149.5	0.99	0.21	1×10^{-7}	0.98	0	127

TABLE IX

SUMMARY STATISTICS OF NOPs DISTRIBUTION IN INDOOR LOCATIONS- (COMPATIBLE WITH PYTHON SCIPY.STATS LIBRARY)

Scenario	Location	Distribution	KS Stat	p-value	
LOS	Sello	Normal	0.22	0.34	
		Exponential	0.28	0.12	
		Log-Normal	0.15	0.76	
		Rayleigh	0.19	0.52	
		Rician	0.19	0.52	
		Nakagami	0.19	0.52	
		Gamma	0.167	0.71	
		Beta	0.167	0.71	
		Log Logistic	0.127	0.92	
		Airport	Normal	0.19	0.79
			Exponential	0.19	0.8
			Log-Normal	0.45	0.02
	Rayleigh		0.19	0.79	
	Rician		0.19	0.79	
	Nakagami		0.25	0.44	
	TUAS	Gamma	0.26	0.404	
		Beta	0.19	0.76	
		Log Logistic	0.162	0.92	
		TUAS2	Normal	0.15	0.67
			Exponential	0.15	0.67
			Log-Normal	0.42	7×10^{-7}
	Rayleigh		0.11	0.9	
	Rician		0.11	0.89	
	Nakagami		0.19	0.38	
Gamma	0.35		0.006		
Beta	0.24		0.143		
Log Logistic	0.513		1×10^{-5}		
NLOS	TUAS2		Normal	0.136	0.189
			Exponential	0.118	0.33
			Log-Normal	0.106	0.46
		Rayleigh	0.154	0.099	
		Rician	0.154	0.099	
		Nakagami	0.072	0.88	
	Gamma	0.093	0.62		
	Beta	0.093	0.62		
	Log Logistic	0.56	8×10^{-19}		

TABLE X

SUMMARY STATISTICS OF MPCs DISTRIBUTION IN OUTDOOR LOCATIONS- (COMPATIBLE WITH PYTHON SCIPY.STATS LIBRARY)

scenario	Location	Distribution	KS Stat	p-value		
LOS	Campus	Normal	0.18	0.17		
		Exponential	0.18	0.17		
		Log-Normal	0.40	1×10^{-5}		
		Rayleigh	0.15	0.34		
		Rician	0.15	0.34		
		Nakagami	0.13	0.54		
		Gamma	0.10	0.8		
		Beta	0.10	0.8		
		Log Logistic	0.09	0.86		
		Residential	Normal	0.22	0.14	
			Exponential	0.13	0.7	
			Log-Normal	0.09	0.96	
	Rayleigh		0.25	0.05		
	Rician		0.25	0.05		
	Nakagami		0.26	0.05		
	NLOS	City	Gamma	0.154	0.53	
			Beta	0.11	0.85	
			Log Logistic	0.091	0.97	
			Residential	Normal	0.15	0.53
				Exponential	0.181	0.34
				Log-Normal	0.625	5×10^{-10}
				Rayleigh	0.139	0.66
				Rician	0.139	0.66
				Nakagami	0.31	0.013
Residential			Gamma	0.233	0.11	
			Beta	0.22	0.121	
			Log Logistic	0.191	0.28	
		Residential	Normal	0.17	0.086	
			Exponential	0.34	2×10^{-5}	
			Log-Normal	0.34	2×10^{-5}	
			Rayleigh	0.23	0.013	
			Rician	0.22	0.013	
			Nakagami	0.404	1×10^{-7}	
		Gamma	0.36	5×10^{-6}		
		Beta	0.34	2×10^{-5}		
		Log Logistic	0.34	2×10^{-5}		

REFERENCES

- [1] H. Wymeersch, D. Shrestha, C. M. De Lima, V. Yajnanarayana, B. Richerzhagen, M. F. Keskin, K. Schindhelm, A. Ramirez, A. Wolfgang, M. F. De Guzman *et al.*, "Integration of communication and sensing in 6G: A joint industrial and academic perspective," in *Proc. PIMRC*. IEEE, 2021, pp. 1–7.
- [2] B. De Beelde, D. Plets, C. Desset, E. Tanghe, A. Bourdoux, and W. Joseph, "Material characterization and radio channel modeling at D-Band frequencies," *IEEE Access*, vol. 9, pp. 153 528–153 539, 2021.
- [3] M. Wang, Y. Wang, W. Li, J. Ding, C. Bian, X. Wang, C. Wang, C. Li, Z. Zhong, and J. Yu, "Reflection characteristics measurements of indoor wireless link in D-Band," *MDPI Sensors*, vol. 22, no. 18, p. 6908, 2022.
- [4] M. A. Aliouane, J.-M. Conrat, J.-C. Cousin, and X. Begaud, "Material reflection measurements in centimeter and millimeter wave ranges for 6G wireless communications," in *EuCNC/6G Summit*, 2022, pp. 43–48.
- [5] —, "Indoor material transmission measurements between 2 GHz and 170 GHz for 6G wireless communication systems," in *Proc. EuCAP*, 2022, pp. 1–5.
- [6] S. Kim, W. T. Khan, A. Zajić, and J. Papapolymerou, "D-Band channel measurements and characterization for indoor applications," *IEEE Trans. Antennas Propag.*, vol. 63, no. 7, pp. 3198–3207, 2015.
- [7] L. Pometcu and R. D'Errico, "An indoor channel model for high data-rate communications in D-Band," *IEEE Access*, vol. 8, pp. 9420–9433, 2020.
- [8] V. Petrov, A. Pyattaev, D. Moltchanov, and Y. Koucheryavy, "Terahertz band communications: Applications, research challenges, and standardization activities," in *ICUMT*. IEEE, 2016, pp. 183–190.
- [9] J. Kokkonen, V. Petrov, D. Moltchanov, J. Lehtomaeki, Y. Koucheryavy, and M. Juntti, "Wideband terahertz band reflection and diffuse scattering measurements for beyond 5G indoor wireless networks," in *EW*, 2016, pp. 1–6.
- [10] C. Han, Y. Wang, Y. Li, Y. Chen, N. A. Abbasi, T. Kürner, and A. F. Molisch, "Terahertz wireless channels: A holistic survey on measurement, modeling, and analysis," *IEEE Commun. Surveys Tuts.*, vol. 24, no. 3, pp. 1670–1707, 2022.
- [11] C.-F. Yang, B.-C. Wu, and C.-J. Ko, "A ray-tracing method for modeling indoor wave propagation and penetration," *IEEE Trans. Antennas Propag.*, vol. 46, no. 6, pp. 907–919, 1998.
- [12] H.-W. Son and N.-H. Myung, "A deterministic ray tube method for microcellular wave propagation prediction model," *IEEE Trans. Antennas Propag.*, vol. 47, no. 8, pp. 1344–1350, 1999.
- [13] M. Lecci, M. Polese, C. Lai, J. Wang, C. Gentile, N. Golmie, and M. Zorzi, "Quasi-deterministic channel model for mmwaves: Mathematical formalization and validation," in *GLOBECOM*. IEEE, 2020, pp. 1–6.
- [14] A. Maltsev, A. Pudevay, I. Karls, I. Bolotin, G. Morozov, R. Weiler, M. Peter, and W. Keusgen, "Quasi-deterministic approach to mmwave channel modeling in a non-stationary environment," in *2014 IEEE Globecom Workshops (GC Wkshps)*. IEEE, 2014, pp. 966–971.
- [15] Q. Zhu, C.-X. Wang, B. Hua, K. Mao, S. Jiang, and M. Yao, "3GPP TR 38.901 channel model," in *GLOBECOM*. Wiley Press Hoboken, NJ, USA, 2021, pp. 1–35.
- [16] A. A. Saleh and R. Valenzuela, "A statistical model for indoor multipath propagation," *IEEE J.Sel. Areas Commun.*, vol. 5, no. 2, pp. 128–137, 1987.
- [17] C. Gustafson, K. Haneda, S. Wyne, and F. Tufvesson, "On mm-wave multipath clustering and channel modeling," *IEEE Trans. Antennas Propag.*, vol. 62, no. 3, pp. 1445–1455, 2013.
- [18] J.-H. Park, Y. Kim, Y.-S. Hur, K. Lim, and K.-H. Kim, "Analysis of 60 GHz band indoor wireless channels with channel configurations," in *Proc. PIMRC*, vol. 2. IEEE, 1998, pp. 617–620.
- [19] S. Ju and T. S. Rappaport, "Statistical channel model of wideband sub-THz radio propagation in indoor factories at 142 GHz: Towards 6G industrial wireless networks," *IEEE Trans. on Wireless Comm.*, pp. 1–1, 2024.
- [20] C. Weragama, J. Kokkonen, M. F. De Guzman, K. Haneda, P. Kyosti, and M. Juntti, "Characterization of spatial-temporal channel statistics from indoor measurement data at D Band," *arXiv preprint arXiv:2403.18713*, 2024.
- [21] M. F. De Guzman and K. Haneda, "Comparison of indoor propagation channels at 28 GHz and 140 GHz bands," in *Proc. European Conf. Antennas Propag.* IEEE, 2024, pp. 1–5.
- [22] S. Hur, S. Baek, B. Kim, Y. Chang, A. F. Molisch, T. S. Rappaport, K. Haneda, and J. Park, "Proposal on millimeter-wave channel modeling for 5G cellular system," *IEEE J. Sel. Topics Signal Process.*, vol. 10, no. 3, pp. 454–469, 2016.
- [23] Y. Chang, S. Baek, S. Hur, Y. Mok, and Y. Lee, "A novel dual-slope mm-Wave channel model based on 3D ray-tracing in urban environments," in *Proc. PIMRC*, 2014, pp. 222–226.
- [24] H. Tataria, K. Haneda, A. F. Molisch, M. Shafi, and F. Tufvesson, "Standardization of propagation models for terrestrial cellular systems: A historical perspective," *Int. J. Wireless Inf. Netw.*, vol. 28, pp. 20–44, 2020.
- [25] K. Haneda *et al.*, "Indoor 5G 3GPP-like channel models for office and shopping mall environments," in *Proc. ICC*, 2016, pp. 694–699.
- [26] S. Das, D. Sen, E. Viterbo, A. K. R. Chavva, D. Sharma, and A. Nigam, "Ambit-process-based spatial-wideband MIMO channel model for sub-THz urban microcellular communication," *IEEE Trans. Wireless Commun.*, vol. 23, no. 1, pp. 559–574, 2024.
- [27] N. T. Nguyen, M. Ma, O. Lavi, N. Shlezinger, Y. C. Eldar, A. L. Swindlehurst, and M. Juntti, "Deep unfolding hybrid beamforming designs for THz massive MIMO systems," *IEEE Trans. Signal Proc.*, vol. 71, pp. 3788–3804, 2023.
- [28] N. T. Nguyen, N. Shlezinger, Y. C. Eldar, and M. Juntti, "Multiuser MIMO wideband joint communications and sensing system with sub-carrier allocation," *IEEE Trans. Signal Proc.*, vol. 71, pp. 2997–3013, 2023.
- [29] M. F. De Guzman, P. Koivumäki, and K. Haneda, "Double-directional multipath data at 140 GHz derived from measurement-based ray-launcher," in *Proc. VTC-Spring*, 2022, pp. 1–6.
- [30] S. L. H. Nguyen, J. Järveläinen, A. Karttunen, K. Haneda, and J. Putkonen, "Comparing radio propagation channels between 28 and 140 GHz bands in a shopping mall," in *Proc. EuCAP*, 2018, pp. 1–5.
- [31] S. L. H. Nguyen, K. Haneda, J. Järveläinen, A. Karttunen, and J. Putkonen, "Large-scale parameters of spatio-temporal short-range indoor backhaul channels at 140 GHz," in *Proc. VTC-Spring*, 2021, pp. 1–6.
- [32] M. F. de Guzman, K. Haneda, and P. Kyosti, "Measurement-based MIMO channel model at 140 GHz," Mar. 2023. [Online]. Available: <https://doi.org/10.5281/zenodo.7640353>
- [33] D. G. Selimis, M. F. De Guzman, K. N. Manganaris, F. I. Lazarakis, K. Haneda, and K. P. Peppas, "Path loss, angular spread and channel sparsity modeling for indoor and outdoor environments at the sub-thz band," *Physical Communication*, vol. 66, p. 102453, 2024.
- [34] E. N. Papatotiriou, A.-A. A. Boulogeorgos, K. Haneda, M. F. de Guzman, and A. Alexiou, "An experimentally validated fading model for THz wireless systems," *Springer Scientific Reports*, vol. 11, no. 1, pp. 2045–2322, 2021.
- [35] F. J. Massey Jr, "The Kolmogorov-Smirnov test for goodness of fit," *J.American Statistical Assoc.*, vol. 46, no. 253, pp. 68–78, 1951.
- [36] S. Kullback and R. A. Leibler, "On information and sufficiency," *Annals Mathematical Statistics*, vol. 22, no. 1, pp. 79–86, 1951.
- [37] B. Yap and C. Sim, "Power comparison of shapiro-wilk, kolmogorov-smirnov, lilliefors and anderson-darling tests," *J. Stat. Model. Analytics*, vol. 1, pp. 21–33, 2011.
- [38] C. R. Harris, K. J. Millman, S. J. van der Walt, R. Gommers, P. Virtanen, D. Cournapeau, E. Wieser, J. Taylor, S. Berg, N. J. Smith *et al.*, "Array programming with NumPy," *Nature*, vol. 585, no. 7825, pp. 357–362, 2020.
- [39] W. McKinney, "Data structures for statistical computing in python," *Proceedings of the 9th Python in Science Conference*, vol. 445, no. 1, pp. 51–56, 2010.
- [40] P. Virtanen, R. Gommers, T. E. Oliphant, M. Haberland, T. Reddy, D. Cournapeau, E. Burovski, P. Peterson, W. Weckesser, J. Bright, S. J. van der Walt, M. Brett, J. Wilson, K. J. Millman, N. Mayorov, A. R. J. Nelson, E. Jones, R. Kern, E. Larson, C. J. Carey, Í. Polat, Y. Feng, E. W. Moore, J. VanderPlas, D. Laxalde, J. Perktold, R. Cimman, I. Henriksen, E. A. Quintero, C. Harris, A. M. Archibald, A. H. Ribeiro, F. Pedregosa, P. van Mulbregt, and S. . Contributors, "SciPy 1.0: Fundamental Algorithms for Scientific Computing in Python," in *Nature Methods*, vol. 17, 2020, pp. 261–272. [Online]. Available: <https://www.nature.com/articles/s41592-019-0686-2>
- [41] J. D. Hunter, "Matplotlib: A 2D graphics environment," *Computing in Science & Engineering*, vol. 9, no. 3, pp. 90–95, 2007.
- [42] M. L. Waskom, "Seaborn: Statistical data visualization," *Journal of Open Source Software*, vol. 6, no. 60, p. 3021, 2021.
- [43] H. Hashemi, "Impulse response modeling of indoor radio propagation channels," *IEEE J.Sel. Areas Commun.*